



UNIVERSITY OF LEEDS

This is a repository copy of *A high-resolution study of graphite nodule formation in experimental medium-carbon machining steel*.

White Rose Research Online URL for this paper:
<http://eprints.whiterose.ac.uk/119512/>

Version: Accepted Version

Article:

Inam, A, Brydson, R orcid.org/0000-0003-2003-7612 and Edmonds, DV (2017) A high-resolution study of graphite nodule formation in experimental medium-carbon machining steel. *Materials Characterization*, 131. pp. 508-516. ISSN 1044-5803

<https://doi.org/10.1016/j.matchar.2017.07.040>

© 2017 Published by Elsevier Inc. This manuscript version is made available under the CC-BY-NC-ND 4.0 license <http://creativecommons.org/licenses/by-nc-nd/4.0/>

Reuse

Items deposited in White Rose Research Online are protected by copyright, with all rights reserved unless indicated otherwise. They may be downloaded and/or printed for private study, or other acts as permitted by national copyright laws. The publisher or other rights holders may allow further reproduction and re-use of the full text version. This is indicated by the licence information on the White Rose Research Online record for the item.

Takedown

If you consider content in White Rose Research Online to be in breach of UK law, please notify us by emailing eprints@whiterose.ac.uk including the URL of the record and the reason for the withdrawal request.



eprints@whiterose.ac.uk
<https://eprints.whiterose.ac.uk/>

Accepted Manuscript

A high-resolution study of graphite nodule formation in experimental medium-carbon machining steel

A. Inam, R. Brydson, D.V. Edmonds

PII: S1044-5803(17)30359-5
DOI: doi: [10.1016/j.matchar.2017.07.040](https://doi.org/10.1016/j.matchar.2017.07.040)
Reference: MTL 8777
To appear in: *Materials Characterization*
Received date: 8 February 2017
Revised date: 21 July 2017
Accepted date: 23 July 2017



Please cite this article as: A. Inam, R. Brydson, D.V. Edmonds , A high-resolution study of graphite nodule formation in experimental medium-carbon machining steel, *Materials Characterization* (2017), doi: [10.1016/j.matchar.2017.07.040](https://doi.org/10.1016/j.matchar.2017.07.040)

This is a PDF file of an unedited manuscript that has been accepted for publication. As a service to our customers we are providing this early version of the manuscript. The manuscript will undergo copyediting, typesetting, and review of the resulting proof before it is published in its final form. Please note that during the production process errors may be discovered which could affect the content, and all legal disclaimers that apply to the journal pertain.

A High-Resolution Study of Graphite Nodule Formation in Experimental Medium-Carbon Machining Steel

A. Inam ^a, R. Brydson ^b and D.V. Edmonds ^b

^a Department of Metallurgy and Materials Engineering
College of Engineering and Emerging Technologies
University of the Punjab
Quaid-e-Azam Campus
Lahore 54590
Pakistan

^b School of Chemical and Process Engineering
University of Leeds
Leeds, LS2 9JT
United Kingdom

Author email addresses: Aqil Inam [aqil.ceet@pu.edu.pk]; Rik Brydson [mtrlrmb@leeds.ac.uk]; David Edmonds [d.v.edmonds@leeds.ac.uk]

Corresponding Author:

David V Edmonds FREng FIMMM CEng CSci FASM
Professor Emeritus and Visiting Research Professor
School of Chemical and Process Engineering
University of Leeds
Leeds LS2 9JT
United Kingdom

tel: +44 (0)113 343 2426

fax: +44 (0)113 343 2384

email: d.v.edmonds@leeds.ac.uk

Abstract

Alloying a medium-carbon steel has accelerated graphite formation during annealing, for example, during high-temperature tempering. Electron microscopy and related techniques

have been used to characterise the graphite particle structure and dispersion from pre-anneal starting microstructures of ferrite-pearlite, bainite and martensite. Graphitisation in the solid state in steels (and also, for useful comparison, in cast irons) has previously received little attention. However, FIB/FEGSEM has permitted specimen preparation of the relatively coarse microstructures, thus enabling high-resolution observation previously limited for graphite formation in cast irons and steels. The study has importance to the potential development of more economic and user-friendly machining steels, which would rely upon internal lubrication by graphite nodules within the microstructure. Many recently developed advanced steels are reduced in carbon but expensively alloyed to produce the desired properties, whereas an aim in this project is simply to use carbon, which is a very cheap and abundant alloying element.

Keywords: free-machining steel; graphitisation; ferrite/pearlite, bainite, martensite; FIB/FEGSEM; HRTEM.

1. Introduction

Graphite formation during solidification of grey cast iron (flake form) and ductile iron (nodular form) is known as primary graphitisation, which results in a stable graphite-iron structure. Graphite formation in the solid-state by decomposition of metastable iron carbides is called secondary graphitisation [1]. Such solid-state graphitisation is an established process practiced as early as the nineteenth century for producing blackheart iron from white cast irons by decomposing the cementite phase in white cast irons by means of a very long annealing process [2]. Such a solid-state annealing process might prove useful in carbon steels, particularly to produce a graphite dispersion which could provide internal lubrication during finishing by machining [e.g. 3-5]. Current practice to produce specific free-machining (free-cutting) steels is to employ enhanced or special alloying additions (e.g. Pb, S, P, Bi, Se, Te) which presents some difficulties with processing or re-cycling [3, 6-9]. However, fast graphitisation would be required given the necessity of short annealing times in the high tonnage steel industry. Thus it is significant that recent studies have shown accelerated graphitisation after annealing with Si and Al [3,10-12]. A recent detailed light optical and scanning electron microscopy study has documented this accelerated graphitisation in typical pre-anneal starting microstructures of ferrite-pearlite, bainite and martensite; meaningful

differences in the nucleation sites and distribution of graphite particles were found [13]. This paper follows with a higher-resolution examination of the same experimental steel using a variety of electron microscopy techniques, made possible through developments in sample preparation, significantly, in precision ion beam thinning/polishing methods. In addition, a companion paper by different authors focused mainly upon the pre-anneal bainite starting microstructure, but significantly using the same experimental steel composition under the same annealing conditions, has also recently been published [14]. Few high-resolution studies of graphite formation have been made in the past because of probable difficulties associated with sample preparation of a relatively coarse aggregate microstructure. Previous emphasis in materials characterisation has been mainly upon observation at ever-increasing resolution of ever-more refined structure, evidenced recently by the transition from micro to nano. In contrast, the results presented here embody high-resolution techniques (HRTEM) applied to industrially and commercially relevant coarse microstructures enabled by improved sample preparation (FIB/FEGSEM).

2. Material and methods

Details of preparation of the experimental steel studied have been described in reference [13]: a medium-carbon steel containing relatively high Si and Al content made as a 60 kg heat at Tata Steel, Rotherham, UK, with designation 4982 [15] and analysis as given in Table 1. The higher levels of Al and Si, combined with a relatively low Mn content, were designed to enhance the graphitising potential of the experimental steel [10-12].

Table 1 Chemical composition (wt. %) of the experimental steel studied.

Wt. % Element												
C	Si	Mn	P	S	Cr	Mo	Ni	Al	B	Cu	N	Sn
0.39	1.86	0.110	0.010	0.0019	0.005	0.015	0.005	1.38	0.0005	0.005	0.0022	0.0003

Three pre-anneal starting microstructural conditions were produced:

- Ferrite/pearlite (as-received in hot-rolled and normalised condition);
- Bainite (austenitised 1150 °C for 7 min and austempered at 400–420 °C for 60 min in a nitrate salt bath);
- Martensite (austenitised 1150 °C for 7 min and water quenched).

Graphitising heat-treatment was carried out in a Carbolite programmable electrical resistance heating chamber furnace, the same as used for austenitising. Steel specimens were heated to 680 °C at a heating rate ~5 °C/min and annealed for different time periods, prior to cooling in the furnace at a rate of 0.5 °C/min to ambient temperature.

Metallographic specimens prepared for light optical microscopy as described in reference [13] were also used for conventional scanning electron microscopy (SEM) by secondary electron imaging (SEs) and energy dispersive X-ray spectroscopy (EDX) on a LEO 1530 Gemini FEGSEM equipped with Silicon Drift Detector (SDD). Both imaging and EDX analyses were carried out at 10 kV. In addition, a Dual Beam FEI Nova 200 Field Emission Gun Scanning Electron Microscope (FEGSEM) with a focused ion beam (FIB) column was used for preparing FIB lamellas of regions containing graphite particles for subsequent study by high-resolution transmission electron microscopy (HRTEM). The unique advantage of this technique to the current investigation was that it proved to be possible to locate and identify a graphite nodule by SEM imaging and EDX analysis, and then produce a site-specific FIB lamella (approximately 60 nm in thickness) containing the same nodule for examination by high-resolution TEM. TEM was undertaken on an FEI Tecnai TF20 field emission gun TEM/STEM (scanning) transmission electron microscope) fitted with an high angle annular dark field HAADF STEM detector, Oxford Instruments INCA 350 EDX system and Gatan Orius CCD (charged-coupled device) camera operated at 200 kV.

3. Results and Discussion

3.1 SEM observations: General effect of pre-anneal starting microstructure on graphite dispersion

SEM micrographs illustrating the typical starting microstructures of ferrite-pearlite, upper bainite and lath martensite before graphitisation annealing at 680°C for varying times are shown in Fig. 1.

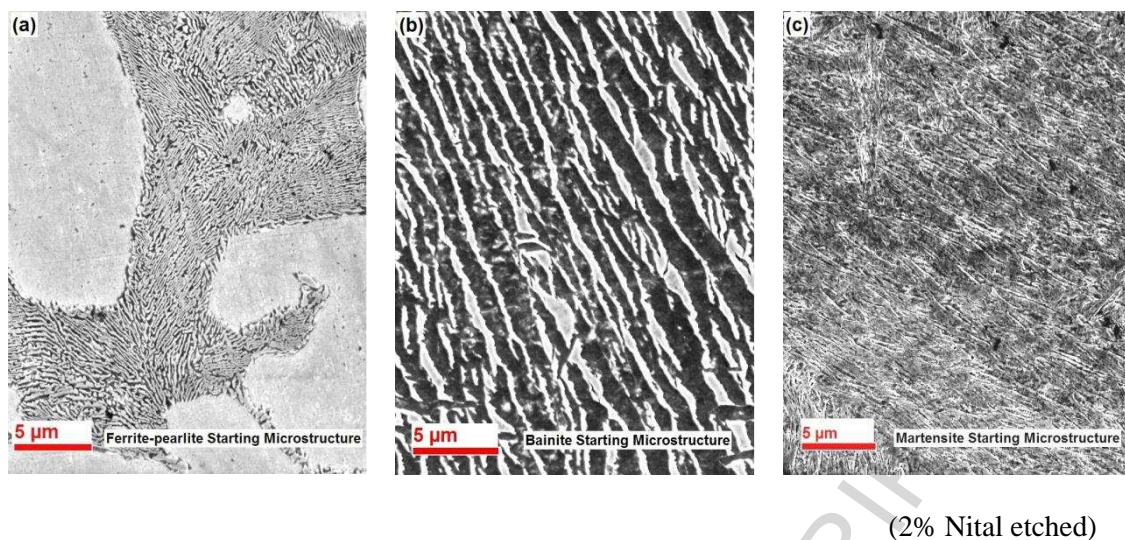
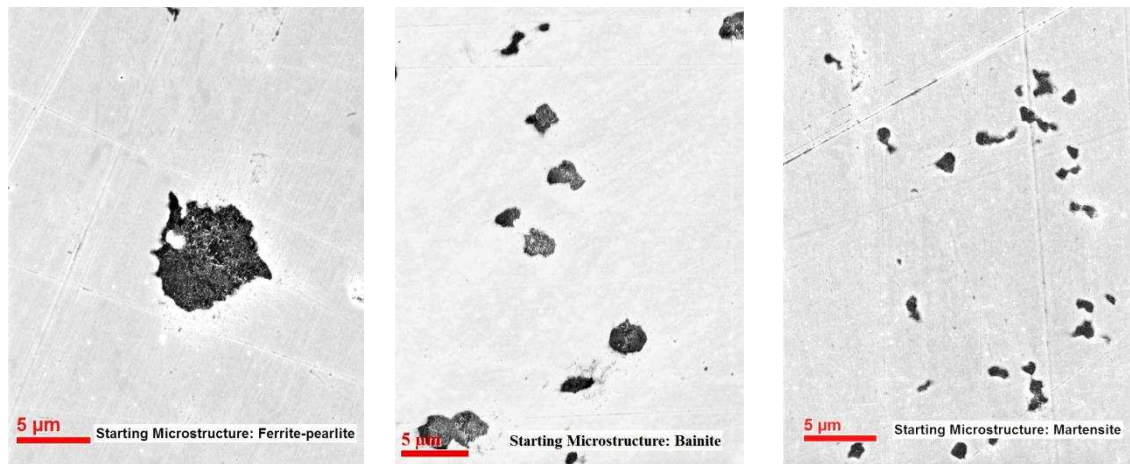
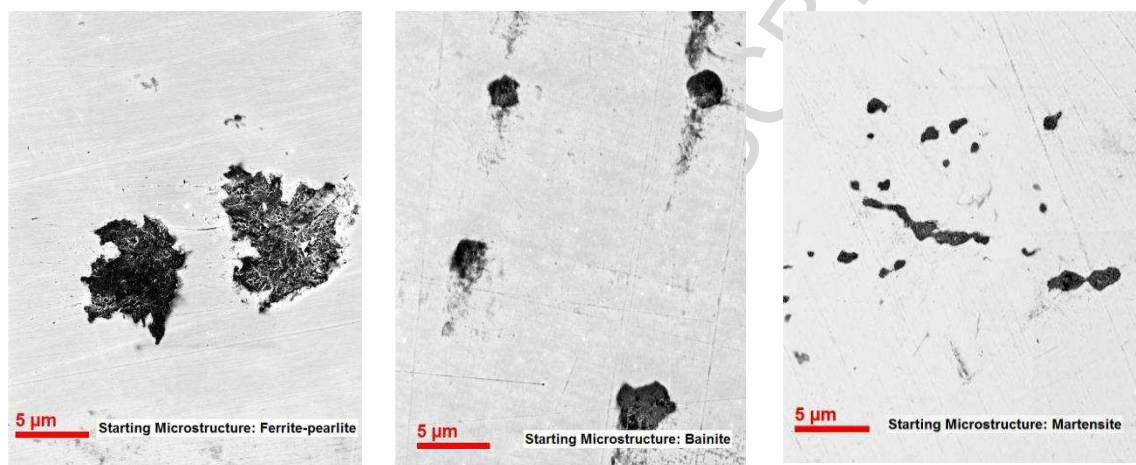


Fig. 1 SEM micrographs of starting microstructures: (a) ferrite-pearlite; (b) upper bainite; and (c) lath martensite.

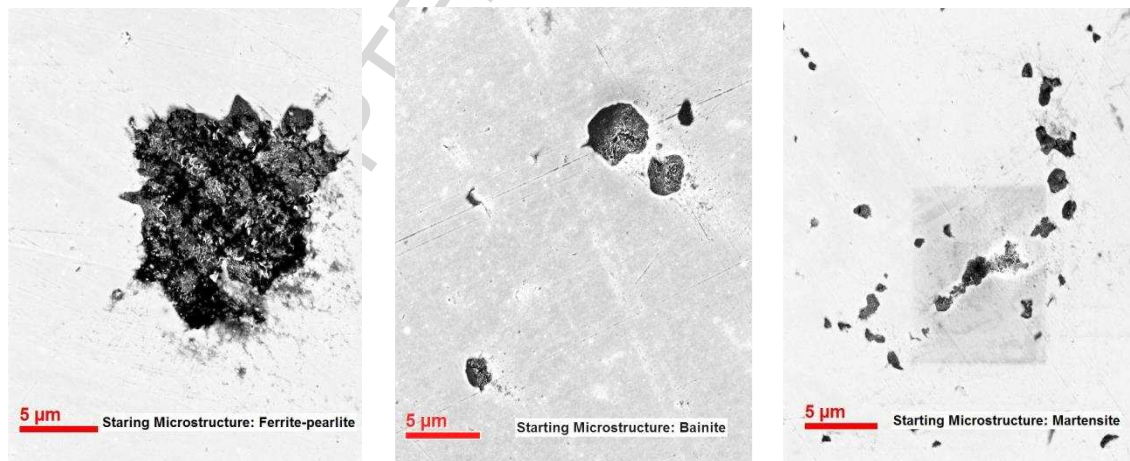
Figures 2 and 3 show a selection of SEM micrographs illustrating the graphite dispersions formed from ferrite-pearlite, bainite, and martensite, after the 680 °C anneal. Carbide particles are generally revealed only after etching, whilst the graphite particles can be seen clearly in both the un-etched (Fig. 2) and etched (Fig. 3) conditions. The particles visible in the un-etched microstructures formed after relatively short times of 20, 30 and 60 minutes of graphitising anneal, presented in Fig. 2, can be identified as graphite. The resolution of the SEM of the un-etched surface can also give a clear picture of the evolution of the graphite nodules. These details of evolution generally appear similar to those identified by light optical microscopy [13], for example, graphite particle morphologies, size and dispersion. There is some evidence for coalescence of the graphite particles (more prevalent for those aligned along grain boundaries) in the martensite starting microstructure, e.g. Fig. 2(b). The SEM micrographs for the etched starting microstructures are presented after longer graphitising anneals at 680 °C for 2, 3 and 5 hours, respectively. An immediate impression from observation of the microstructures after short annealing times compared with longer annealing times is that significant graphite formation occurs relatively rapidly. Further growth after approximately 1-2 hours is not readily apparent and no major changes in dispersion are perceptible.



(a) Graphite dispersion formed after 20 minutes of graphitising anneal.

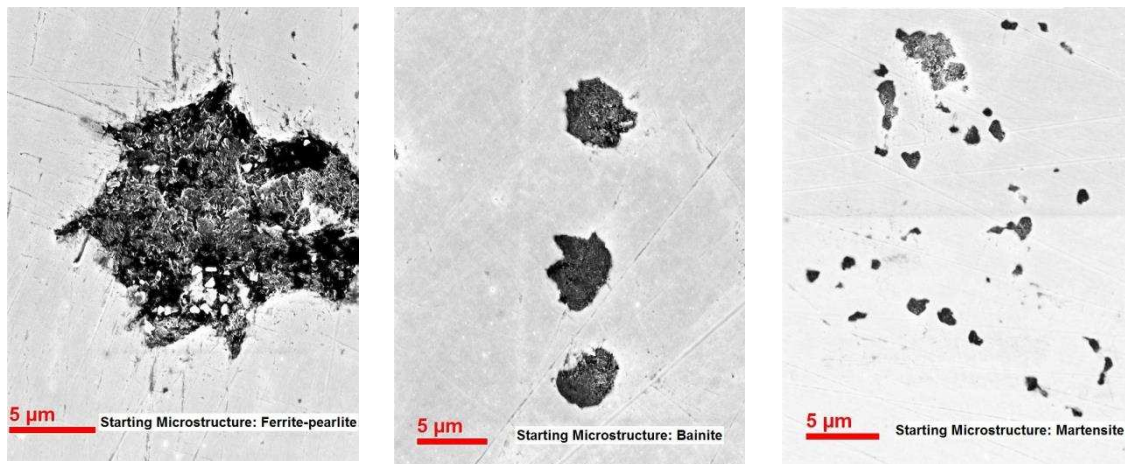


(b) Graphite dispersion formed after 30 minutes of graphitising anneal.

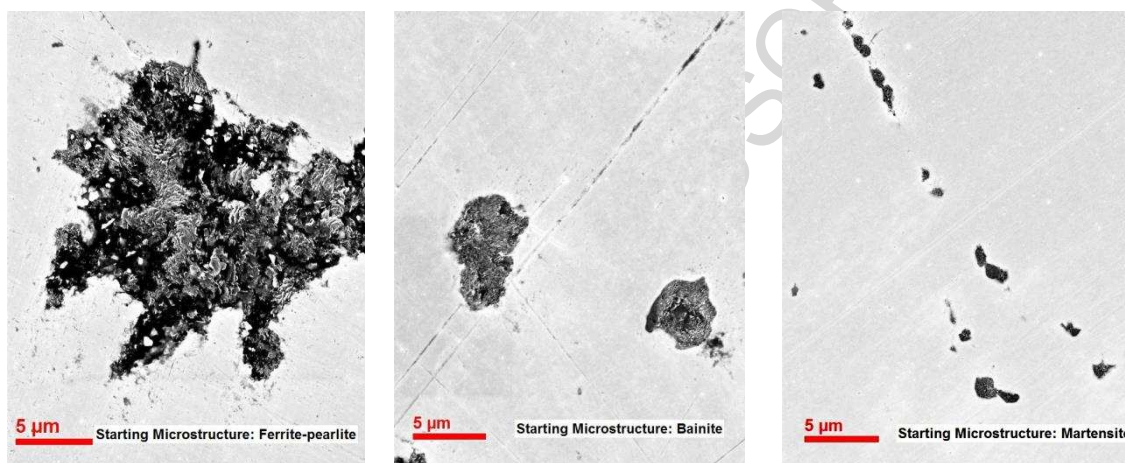


(c) Graphite dispersion formed after 1 hour of graphitising anneal.

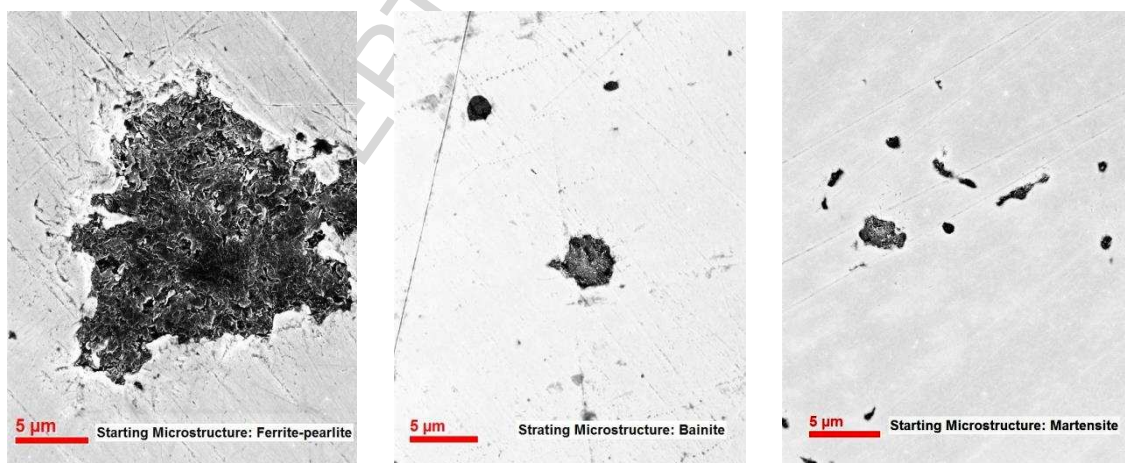
Fig. 2 SEM micrographs (un-etched samples) showing graphite dispersions formed from starting microstructures, ferrite-pearlite, bainite and martensite, after graphitising anneals at 680 °C of 20, 30 and 60 minutes, are presented in (a), (b) and (c), respectively.



(a) Graphite dispersion formed after 2 hours of graphitising anneal.



(b) Graphite dispersion formed after 3 hours of graphitising anneal.



(c) Graphite dispersion formed after 5 hours of graphitising anneal.

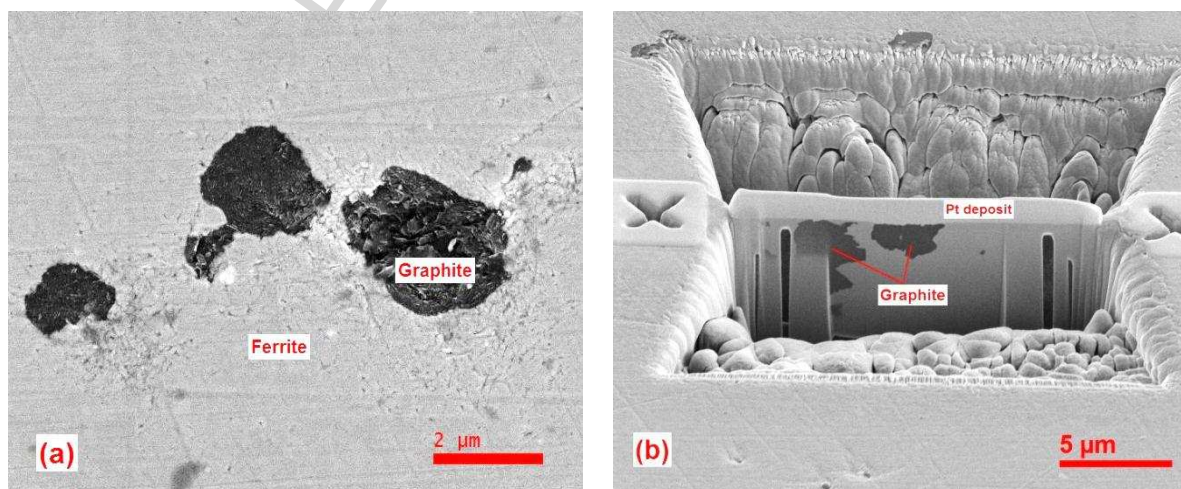
Fig. 3 SEM micrographs (etched samples) showing graphite dispersions formed from starting microstructures, ferrite-pearlite, bainite and martensite, after graphitising anneals of 2, 3 and 5 hours, are presented in (a), (b) and (c), respectively.

The SEM micrographs indicate evidence for increasing size as a function of the pre-anneal starting microstructure and, in the case of nodules forming in the ferrite-pearlite microstructure, accompanying irregularity. Limited measurements of the approximate graphite particle diameters from SEM micrographs are $\leq 20 \mu\text{m}$ (the majority from 10 to 20 μm) for ferrite-pearlite; $\leq 5 \mu\text{m}$ for bainite; $\leq 2 \mu\text{m}$ for martensite pre-anneal starting microstructures.

3.2 HRTEM observations

3.2.1

Figure 4 illustrates the preparation stages of an FIB lamella from a microstructural region containing relatively coarse graphite particles (within an annealed bainitic sample described in detail below). Figure 4(a) shows three graphite particles in a ferrite (formerly more recognisable bainite) matrix; from these the two larger were sliced to form an FIB lamella as shown in Fig. 4(b). After identifying them as graphite particles by SEM EDX analysis, a thin platinum layer was deposited on the lamella in order to avoid any damage or breakage during milling and transfer to a TEM support grid. Figure 4(c) shows the lamella micro-welded to a TEM grid and finally thinned to 57.7 nm thickness indicated by the top-edge view in (Fig. 4(d)).



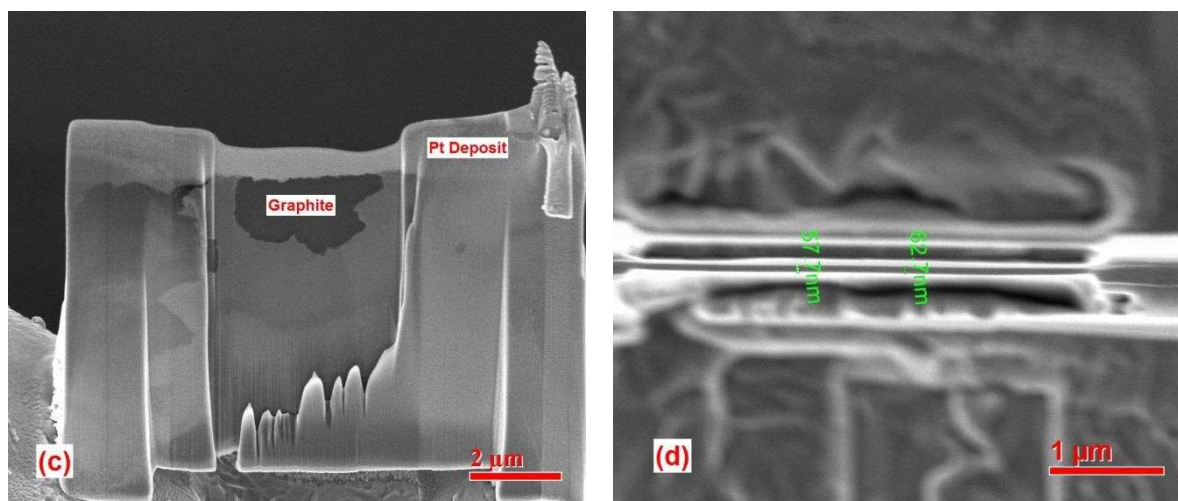
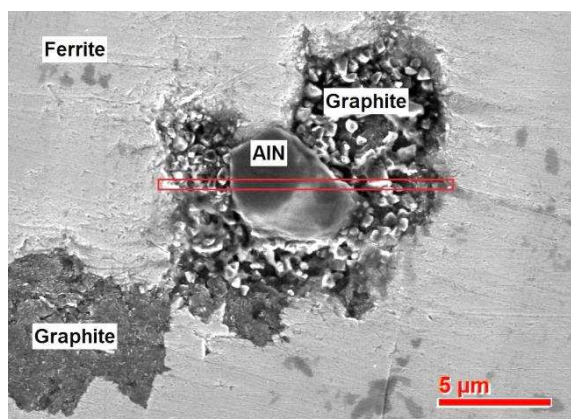


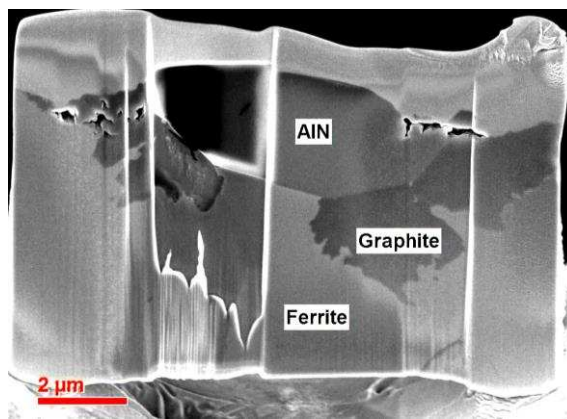
Fig. 4 SEM micrographs showing the preparation stages of an FIB lamella from a microstructural region containing graphite particles: (a) graphite particles in a ferrite matrix, (b) lamella containing graphite particles sliced from the sample by FIB, also showing a supportive Pt deposit, (c) FIB/TEM lamella showing thinned central section suitable for high-resolution TEM, (d) top edge view of thinned FIB/TEM lamella.

3.2.2 Ferrite-pearlite starting microstructure

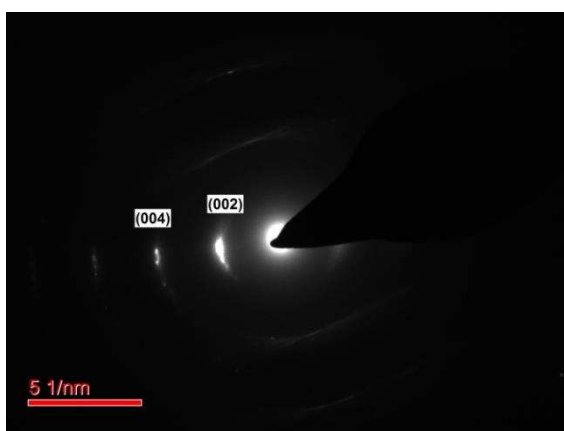
A graphite particle of $\sim 10 \mu\text{m}$ diameter size, formed after 20 minutes of graphitising anneal from the ferrite-pearlite starting microstructure, containing a precipitate particle assumed to have acted as a nucleus, is shown in Fig. 5(a). Irregular graphite nodules apparently nucleated on AlN have previously been observed by He et al. [16]. This heterogeneous nucleation and growth of graphite from AlN has also been examined previously by HRTEM lattice imaging [14,17]. Planarity of the interface at high resolution with a potential degree of coherency between the two lattices has been observed [17]. Figure 5(b) shows a FIB/TEM lamella prepared from the sample region outlined in Fig. 5(a). Figure 5(c) shows a diffraction pattern obtained from the graphite in the FIB/TEM lamella (labelled in Fig. 5(b)). A high-resolution lattice image from this graphite region is shown in Fig. 5(d), and a magnified image from the area outlined, in Fig. 5(e). Figure 5(f) shows the intensity profile of the graphite lattice along the line indicated in Fig. 5(d).



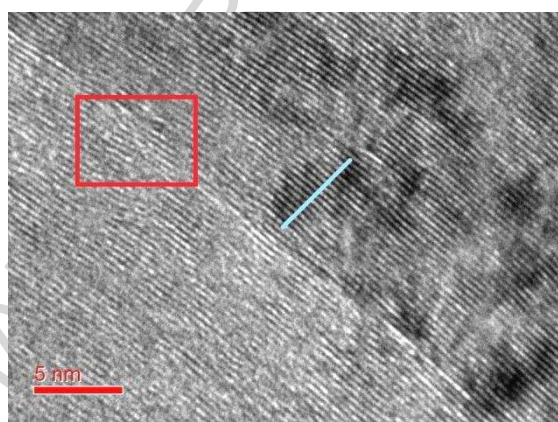
(a) Graphite particle of size $\sim 10 \mu\text{m}$ in diameter containing an AlN precipitate.



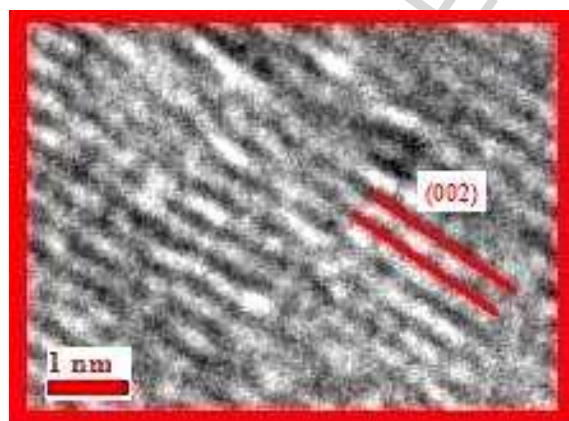
(b) FIB/TEM lamella prepared from region of sample outlined in (a).



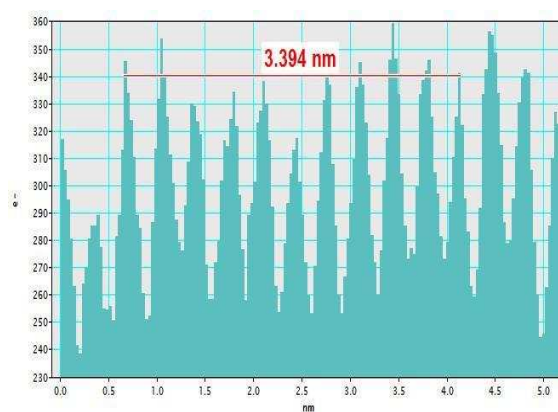
(c) Diffraction pattern from graphite in FIB/TEM lamella in (b).



(d) HRTEM lattice image from graphite in FIB/TEM lamella in (b).



(e) Magnified image from area of graphite outlined in (d).



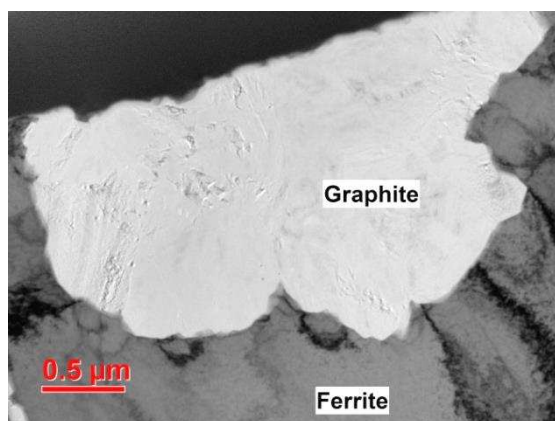
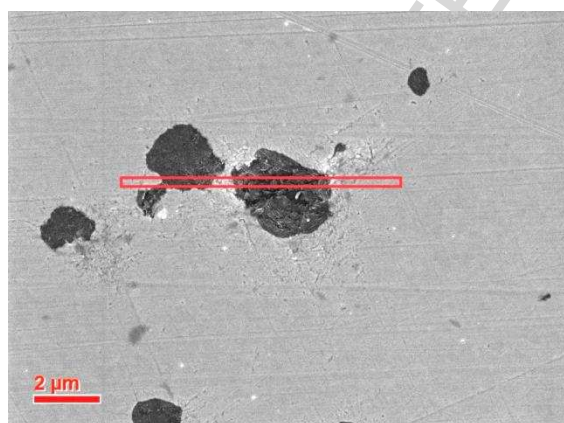
(f) Graphite lattice intensity profile along the line in (d).

Fig. 5 (a) SEM micrograph of a graphite particle formed after 20 minutes of graphitising anneal from ferrite-pearlite starting microstructure and containing an AlN precipitate; (b) FIB/TEM lamella prepared from region of sample outlined in (a); (c) diffraction pattern from graphite in FIB/TEM lamella in (b); (d) HRTEM lattice image from graphite in FIB/TEM lamella in (b); (e) magnified lattice image from area of graphite outlined in (d); (f) graphite lattice intensity profile along the line in (d).

The diffraction pattern in Fig. 5(c) shows strong reflections indexed as (002) and (004), against fairly weak amorphous rings, indicative of crystalline graphite. The HRTEM lattice images of Fig. 5(d) and (e) reveal the graphite (002) planes, which spatially appear straight and parallel, further confirmation of crystallinity. This crystalline regularity is confirmed by the lattice intensity profile of Fig. 5(f), which gives an (002) lattice spacing of 0.339 nm, consistent with figures reported previously for this steel composition by He et al. [16]. This nodule contained a precipitate, identified as AlN, which is most likely to have been the nucleation site. It is noteworthy that this site has been activated after a short annealing time of 20 minutes.

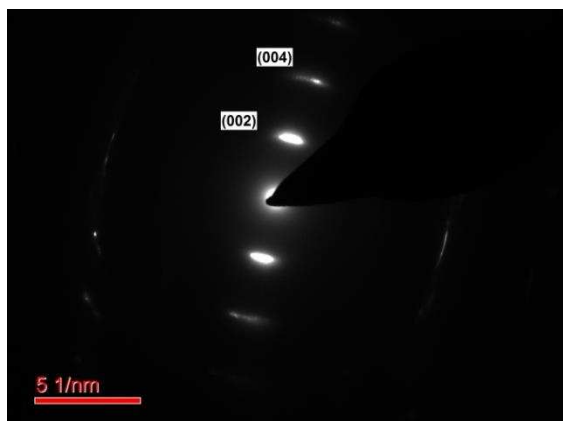
3.2.3 Bainite starting microstructure

The coarser graphite particle, $\sim 3 \mu\text{m}$ diameter, shown already in Fig. 4(a), formed after 20 minutes of graphitising anneal from the bainite starting microstructure, is shown in Fig. 6(a). Figure 6(b) shows the FIB/TEM lamella prepared from the region of this sample outlined in Fig. 6(a). Figure 6(c) shows a diffraction pattern from the graphite. An HRTEM lattice image is shown in Fig. 6(d) and the magnified image from the area outlined in Fig. 6(e). Figure 6(f) records the intensity profile across this image along the line indicated in Fig. 6(d).

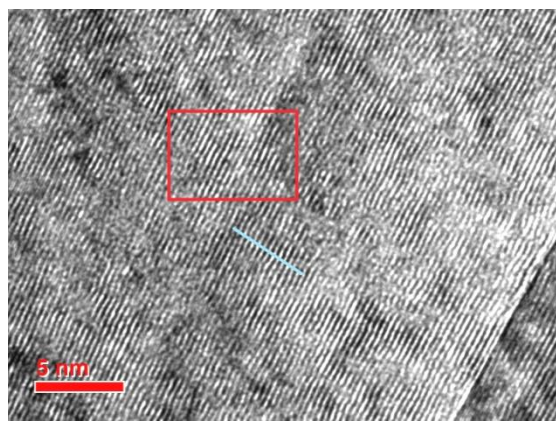


(a) Graphite particle of size $\sim 3 \mu\text{m}$ diameter.

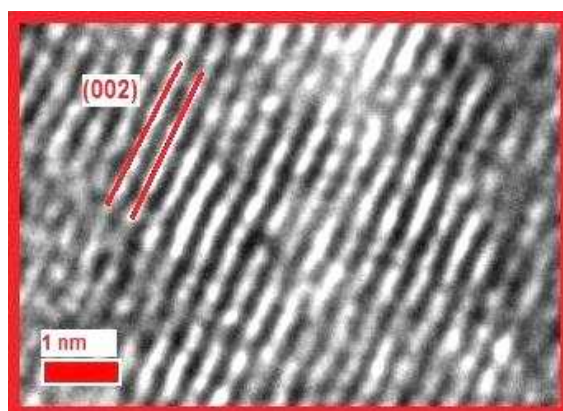
(b) FIB/TEM lamella prepared from region of sample outlined in (a).



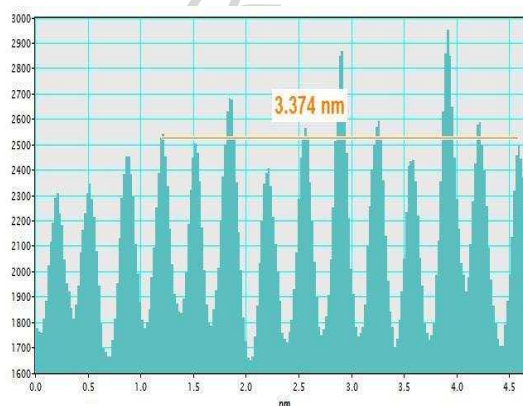
(c) Diffraction pattern from graphite in FIB/TEM lamella in (b).



(d) HRTEM lattice image from graphite in FIB/TEM lamella in (b).



(e) Magnified image from area of graphite outlined in (d).



(f) Graphite lattice intensity profile along the line in (d).

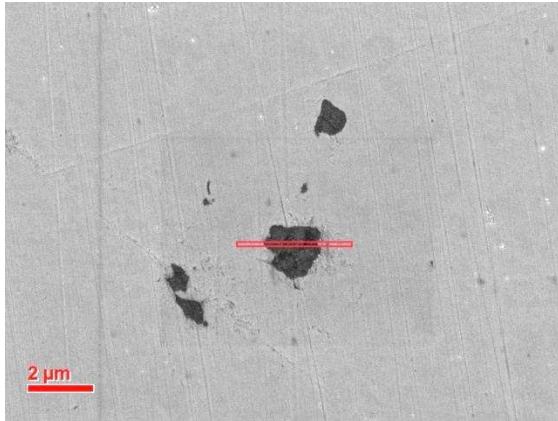
Fig. 6 (a) SEM micrograph of a graphite particle formed after 20 minutes of graphitising anneal from bainite starting microstructure; (b) FIB/TEM lamella prepared from region of sample outlined in (a); (c) diffraction pattern from graphite in FIB/TEM lamella in (b); (d) HRTEM lattice image from graphite in FIB/TEM lamella in (b); (e) magnified lattice image from area of graphite outlined in (d); (f) graphite lattice intensity profile along the line in (d).

HRTEM analysis of this graphite nodule formed from the initial bainite produced results similar to that for the ferrite-pearlite starting microstructure: crystalline graphite with an (002) lattice spacing of 0.337 nm, very close to that measured from the (002) lattice intensity profile for the ferrite-pearlite starting microstructure.

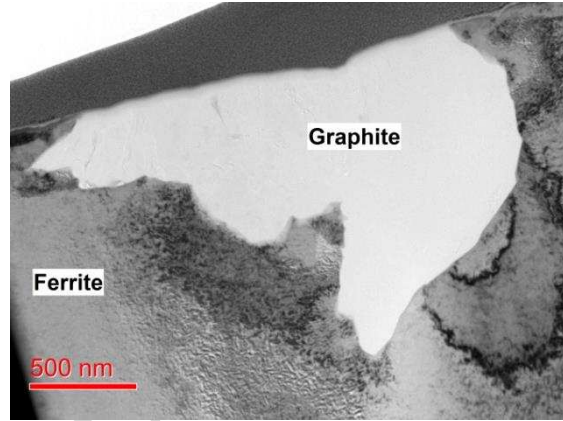
3.2.4 Martensite starting microstructure

A graphite particle $\sim 2 \mu\text{m}$ diameter, formed after 20 minutes of graphitising anneal from the martensite starting microstructure, is shown in Fig. 7(a). Figure 7(b) shows the FIB/TEM

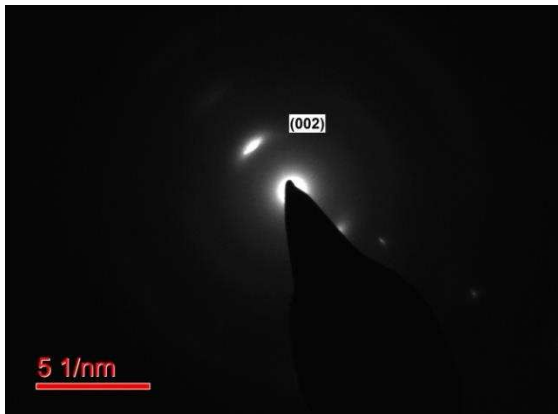
lamella prepared from the sample indicated by the outline in Fig. 7(a). Fig. 7(c) shows a diffraction pattern from the graphite, Fig. 7(d) the HRTEM lattice image of the graphite, Fig. 7(e) a magnified image and Fig. 7(f) the intensity profile across the graphite lattice along the line in Fig. 7(d).



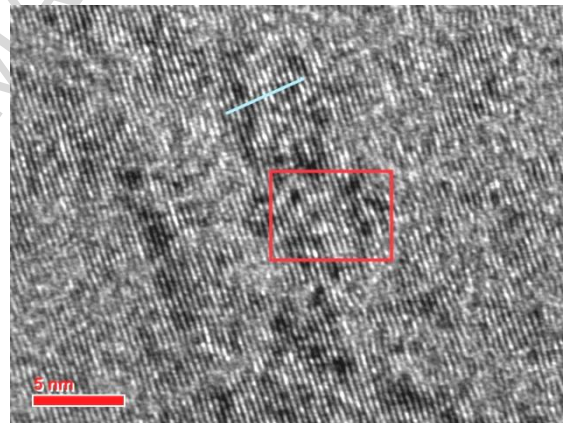
(a) Graphite particle of size $\sim 2 \mu\text{m}$ diameter.



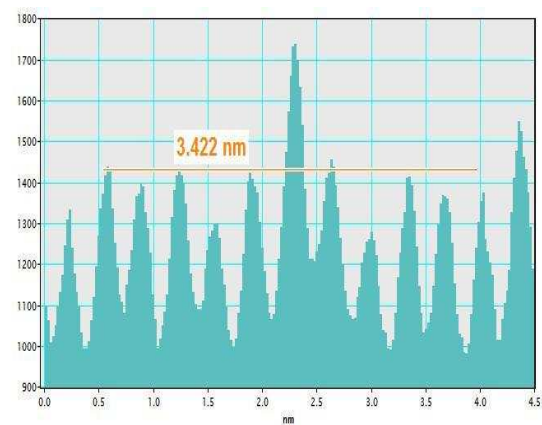
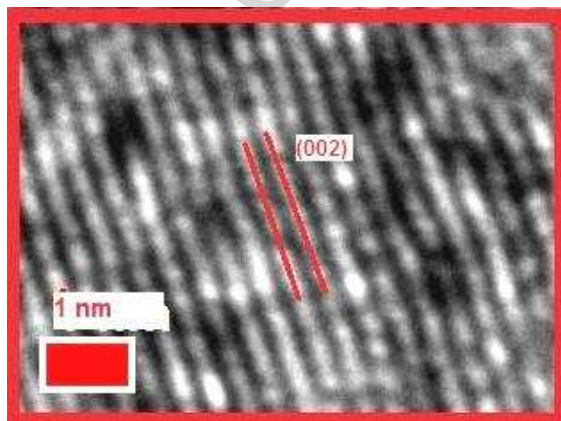
(b) FIB/TEM lamella prepared from region of sample outlined in (a).



(c) Diffraction pattern from graphite in FIB/TEM lamella in (b).



(d) HRTEM lattice image from graphite in FIB/TEM lamella in (b).



- (e) Magnified image from area of graphite outlined in (d). (f) Graphite lattice intensity profile along the line in (d).

Fig. 7 (a) SEM micrograph of a graphite particle formed after 20 minutes of graphitising anneal from martensite starting microstructure; (b) FIB/TEM lamella prepared from region of sample outlined in (a); (c) diffraction pattern from graphite in FIB/TEM lamella in (b); (d) HRTEM lattice image from graphite in FIB/TEM lamella in (b); (e) magnified image from area of graphite outlined in (d); (f) graphite lattice intensity profile along the line in (d).

The results profile of this graphite nodule analysed for the annealed martensitic starting microstructure closely followed those for the other two starting microstructures. HRTEM identified the phase as graphite, formed after 20 minutes of annealing at 680 °C and already with a high degree of crystallinity. In addition, the (002) lattice intensity profile gave an (002) lattice spacing of 0.342 nm.

4. Conclusions

A high-resolution electron microscope study of the coarse graphite dispersion in an experimental carbon steel after annealing has been enabled by focused ion beam (FIB) sample preparation. Thus SEM and HRTEM have been used to identify and record heterogeneous nucleation, graphite particle size, morphology and dispersion, as well as the degree of graphite crystallinity and (002) lattice spacing, following annealing at 680 °C from three different pre-anneal microstructures: ferrite-pearlite, bainite and martensite. The experimental steel was alloyed with Si and Al to accelerate the graphite formation kinetics and some examples have been shown for graphite particles formed after only 20 minutes. It is noteworthy that the degree of crystallinity of the graphite was already well developed after a 20 minute anneal. The rapid graphitisation might enable this experimental steel to be considered as a candidate for free-machining, in which case many of the features and parameters of the graphite, demonstrated in this study to be observable and measurable, even at high resolution, could be useful for optimising the free-machining performance of the microstructure.

Acknowledgements

We are grateful to Tata Steel, Rotherham, UK, for providing the experimental steel for this research work. Aqil Inam is also indebted to the University of the Punjab, Lahore, Pakistan, for financial support whilst undertaking this research project.

References

1. J. Fould, R. Viswanathan, Graphitization of steels in elevated-temperature service, *J. Materials Engineering and Performance*, 2001. **10**(4): p. 484 – 492.
2. I. Minkoff, *The Physical Metallurgy of Cast Iron*, 1983, Chichester: John Wiley and Sons.
3. T. Iwamoto, T. Hoshino, K. Amano, Y. Nakano, An advanced high strength graphitised steel for machining and cold forging uses, in: C.J. Van Tyne, G. Krauss, D.K. Matlock (Eds.), *Fundamentals and Applications of Microalloying Forging Steels*, TMS/Minerals, Metals and Materials Society, Warrendale, PA 1996, pp. 277–286.
4. K. Oikawa, T. Abe, S. Sumi, Medium-carbon steel having dispersed fine graphite structure and method for the manufacture thereof. Patent 6174384, United States of America, 2001.
5. R. Tanaka, Y. Yamane, K. Sekiyab, N. Narutakib, T. Shiragac, Machinability of BN free machining steel in turning, *Int. J. Mach. Tools Manuf.* 47 (2007) 1971–1977.
6. S.R. Lampman, T.B. Zorc, *Properties and Selection: Irons, Steels and High Performance Alloys*; Metals Handbook, ASM International, Materials Park, OH, 1990.
7. E.M. Trent, P.K. Wright, *Metal Cutting*, 4th ed. Butterworth-Heinemann, Boston, 2000.
8. T.H.C. Childs, K. Maekawa, T. Obikawa, Y. Yamane, *Metal Machining: Theory and Applications*, Arnold, London, 2000.
9. T. Akasawa, M. Sakurai, M. Nakamura, T. Tanaka, K. Takano, Effects of free-cutting additives on the machinability of austenitic stainless steels, *Mater. Proc. Technol.* 143–144 (2003) 66–71.
10. K. He, D.V. Edmonds, Acceleration of graphitisation in carbon steels to improve machinability, *Proceedings: Super-high Strength Steels*, 2005, Rome, Associazione Italiana di Metallurgia (AIM)/Centro Sviluppo Materiali (CSM), ISBN: 88-85298-56-7, (CD-ROM) 9 pages, 2005.
11. K. He, D.V. Edmonds, A potential graphitization route to improved machinability of carbon steels, *International Conference on New Developments in Long and Forged Products: Metallurgy and Applications*, June 4-7, 2006, Winter Park, Colorado, USA, Association for Iron & Steel Technology AIST, 2006, pp. 191-202.
12. D.V. Edmonds, K. He, Graphitisation as a potential route to improved machinability of

carbon steels, 61st ABM Annual Congress, Rio de Janeiro, Brazil; 2006, Associação Brasileira de Metalurgia, Materiais e Mineração (ABM), Sao Paulo 2006, pp. 2535–2544.

13. A. Inam, R. Brydson, D.V. Edmonds, Effect of starting microstructure upon the nucleation sites and distribution of graphite particles during a graphitising anneal of an experimental medium-carbon machining steel, *Mater. Char.*, 106 (2015) 86-92.

14. J.X. Gao, B.Q. Wei, D.D. Li, K. He, Nucleation and growth characteristics of graphite spheroids in bainite during graphitization annealing of a medium carbon steel, *Mater. Char.*, 118 (2016) 1-8.

15. A. Inam, PhD Thesis, University of Leeds, UK, 2013.

16. K. He, H.R. Daniels, A. Brown, R. Brydson, D.V. Edmonds, An electron microscopic study of spheroidal graphite nodules formed in a medium-carbon steel by annealing, *Acta Mater.*, 55 (2007) 2919–2927.

17. A. Inam, D.V. Edmonds, R. Brydson, Heterogeneous nucleation of graphite in carbon steel, 15th European Microscopy Congress, Manchester, UK, 2012, D.J. Stokes, W.M. Rainforth (Eds.), Royal Microscopical Society, Oxford, 2012.

Highlights

- HREM of formation of graphite particles in experimental carbon steel alloyed to accelerate kinetics of graphitisation.
- Hence the potential for using graphite in steel as an internal lubricant during machining.
- Influence of pre-anneal starting microstructure on graphite particle morphology, size, distribution and degree of crystallinity, key microstructural parameters likely to influence machinability.
- Potential benefit is new economic and process-friendly recyclable free-cutting simple carbon steel compositions without e.g. Pb alloying.